IEEE Access
Multidisciplinary ⋮ Rapid Review ⋮ Open Access Journal

Received March 4, 2022, accepted March 25, 2022, date of publication March 30, 2022, date of current version April 8, 2022.

Digital Object Identifier 10.1109/ACCESS.2022.3163308

Assessment of Delamination Under Insulation Using Ridge Waveguide

MUHAMMAD FIRDAUS AKBAR[1], (Member, IEEE), NAWAF H. M. M. SHRIFAN[1,2], GHASSAN N. JAWAD[3], (Member, IEEE), AND NOR ASHIDI MAT ISA[1]

[1]School of Electrical and Electronic Engineering, Universiti Sains Malaysia, Nibong Tebal, Penang 14300, Malaysia
[2]Faculty of Oil and Minerals, University of Aden, Aden, Yemen
[3]Department of Electronics and Communications Engineering, University of Baghdad, Baghdad 10071, Iraq

Corresponding authors: Muhammad Firdaus Akbar (firdaus.akbar@usm.my) and Nawaf H. M. M. Shrifan (nawaf_83@hotmail.com)

This work was supported by the Ministry of Education Malaysia Fundamental Research Grant Scheme (FRGS) under Grant FRGS/1/2019/TK04/USM/02/4.

ABSTRACT Insulation has been widely used to protect metal substrates in various industries such as turbine blades and oil and gas pipelines. Due to aging and cyclic processes, delamination between the metal component and insulation could grow. Such defects represent a critical problem that may result in catastrophic failure of the asset. Therefore, detecting and evaluating delaminated areas is mandatory for providing urgent maintenance solutions before the failure occurrence. In this paper, microwave non-destructive technique (NDT) is proposed for delamination detection and thickness estimation under dielectric insulation. In microwave NDT, the electromagnetic waves are induced into the dielectric material's surface using a ridge waveguide. The complex reflection coefficients are acquired using a vector network analyzer for further analysis in the time domain. Next, a time-domain reflectometry (TDR) technique-based inverse discrete Fourier transform is used to evaluate the complex reflection coefficients in terms of delamination's size and thickness estimation. The delamination evaluation is performed by measuring the maximum peak's time-step variations instead of the magnitude reduction in conventional TDR techniques in terms of the defect and defect-free reflections. Next, a comparison is made between implementing the proposed technique using a ridge waveguide and a regular rectangular waveguide. The results prove the superiority of using the ridge waveguide for delamination evaluation in terms of sizing and thickness with a minimum error rate of 5% and 7.87%, respectively. These novel results of ridge waveguide due to its small aperture and relatively wide bandwidth. The microwave NDT technique reported here could provide a predictive maintenance tool for many industries to minimize the maintenance effort and cost.

INDEX TERMS Defect under insulation, delamination, microwave NDT, ridge waveguide, predictive maintenance.

I. INTRODUCTION

Insulations are commonly used to protect the metal substrate in various critical structures, particularly protecting turbine blades in aerospace and power generation industries [1] and the pipelines in the oil and gas industry [2]. Many factors affect the well joining of the metal coated with dielectric insulation in services such as corrosion, air gap, and delamination due to the aging and operation process. Underneath delamination located between the insulation and the metal substrate may occur catastrophic failure of the system structure in many critical applications, especially in aircraft and oil production. These critical applications' failure leads to endangering human life, environmental pollution, and higher maintenance cost.

An accurate analytical inspection using the non-destructive testing (NDT) technique to reveal and evaluate the under-insulation delamination is needed for preventing catastrophic accidents [3]. The accurate non-destructive inspection evaluates the safety and health of the structures without removing the insulation material. The evaluation of the delamination severity in terms of size and depth is mandatory for human safety and environment integrity, reduces the maintenance cost, and enhances the operating system components. Also, a maintenance tool such as NDT can provide helpful information about reaching the delamination

The associate editor coordinating the review of this manuscript and approving it for publication was Xiaokang Yin.

to a critical limit for deciding whether to replace or keep the insulations.

In the past decades, several conventional NDT methods have been developed for delamination evaluation under insulation, such as vibration [4], Lamb waves techniques [5], [6], laser ultrasonic [7], infrared thermography [8], and terahertz NDT [9]–[11]. These conventional techniques have shown promising results in delamination detection due to the research development process and well standardization over the past decades. However, the accurate delamination evaluation in terms of size and depth is the main limitation of the techniques, as mentioned earlier, due to the penetration challenge of inspecting the dielectric materials. A complex computation process is required for interpreting the backscattering Lamb waves because of the higher intersection of the forward and backward waves generated from the sample back-walls, especially in case of multiple defects presence. [12]. Several waves are generated in terms of laser ultrasonic, such as shear, longitudinal waves, rayleigh, and lamb waves make the defect evaluation challenge [13]. The thermography NDT sensitivity is degraded to detect in-depth defects and limited to near-surface heating [14]. In terahertz NDT, generating the radiations in low power degrades the delamination evaluation accurately besides the technology equipment's higher cost [15]. As presented in [15], hybridizing various NDT techniques is expensive and computation complex due to the variations in the utilized equipment and the processing time added by every single technique.

In contrast to conventional NDT, microwave NDT has recently emerged as a promising technique for evaluating the underneath defect in dielectric materials [16]. The induced electromagnetic waves at microwave frequencies (e.g. 18GHz – 40 GHz) can interact appropriately with the inner structure of dielectric insulation [17], [18]. The reflected and transmitted signals are capable of providing helpful information for evaluating underneath delamination. Microwave NDT provides many advantages that do not require a couplant material, a controlled environment or complicated post signal processing. Microwave NDT performs non-contact inspection, operator-friendly, and relatively inexpensive one-sided inspection [19]. Furthermore, a microwave open-ended waveguide can perform remote inspection of anisotropic materials [20] due to the electric field's polarization linearity inside the waveguide, simplifying the signal processing.

Various microwave NDT techniques have been proposed for underneath defect evaluation [21]–[26]. In [21], an open-ended waveguide that depends on the phase profile is proposed to measure the delamination in terms of detection and thickness variations of the composite structure. In [22], the change in the form of permittivity of a composite structure based on the shift in the resonant frequency of the split-ring resonator is demonstrated to image the defects in the GFRP layer. In [23], electromagnetic scanning is performed using a couple of spiral inductors. The variations in the transmission coefficients' magnitude are employed to reveal the abnormalities of the delamination in a composite structure. However, these approaches have shown numerous limitations in thickness estimation accuracy [21] and poor spatial resolution [22], [23] make the estimation of delamination severity challenging.

In microwave NDT, under insulation delamination evaluation is performed by measuring and interpreting the variations in the reflected electric field propagated in the microwave probe aperture during the inspection of the insulation structure. OERW microwave probe is commonly used for defect evaluation in composite materials due to the promising results in terms of delamination detection, sizing, and depth estimation. In [27], principal component analysis (PCA) and synthetic aperture radar (SAR) tomography, including time of flying, are used to analyze microwave OERW response for defect evaluation in GFRP pipe. The technique successfully represents the defect location, shape and depth based on adjusting a threshold. Besides the computational complexity challenge in [28], SAR-based singular value decomposition (SVD) and rang-Doppler algorithm (RDA) have shown promising results in terms of the high resolution of microwave imaging with a 40 mm stand-off distance. However, intensive knowledge is required to select reasonable PCA and SVD components and the threshold value for reliable defect evaluation.

Recently, microwave OERW probe provides noticeable results in inspecting composite materials in terms of defect detection, sizing, and depth estimation, such as machine learning-based techniques [17], [20], [29], [30] and time-domain reflectometry (TDR) [31]. However, the detected delamination's size and depth seem larger than the actual ones. In conventional OERW, the electric field is distributed along with the large aperture in the form of a sine curve in the dominant mode as shown in Figure 1(a). The variations in the electric field smoothly occur once the defect starts confronting the probe aperture. These variations reach their maximum once the defect confronts the middle of the probe aperture. As a result, a large defect size is produced due to the defect is confronting the wide aperture longwise during the spatial inspection. Therefore, a small size of probe aperture operated in a larger bandwidth is preferable for better spatial resolution [32].

In this research, a ridge waveguide is used for performing the material inspection due to its wide measurement bandwidth compared to a rectangular waveguide [33]–[36]. The ridge waveguide is quietly similar to the rectangular waveguide with ridges along the horizontal sides [37]. The electric field in the dominant mode is distributed in the small aperture between the ridges, as shown in Figure 1(b). This focal distribution in the small area is useful for the accurate measurement of lateral defect size. The electric field's significant variations suddenly occur once the defect confronts the small area between the ridges only regardless of the overall aperture size. These sudden variations in the electric field produce a sharper defect shape that enhances inspection accuracy. Moreover, the large bandwidth operated

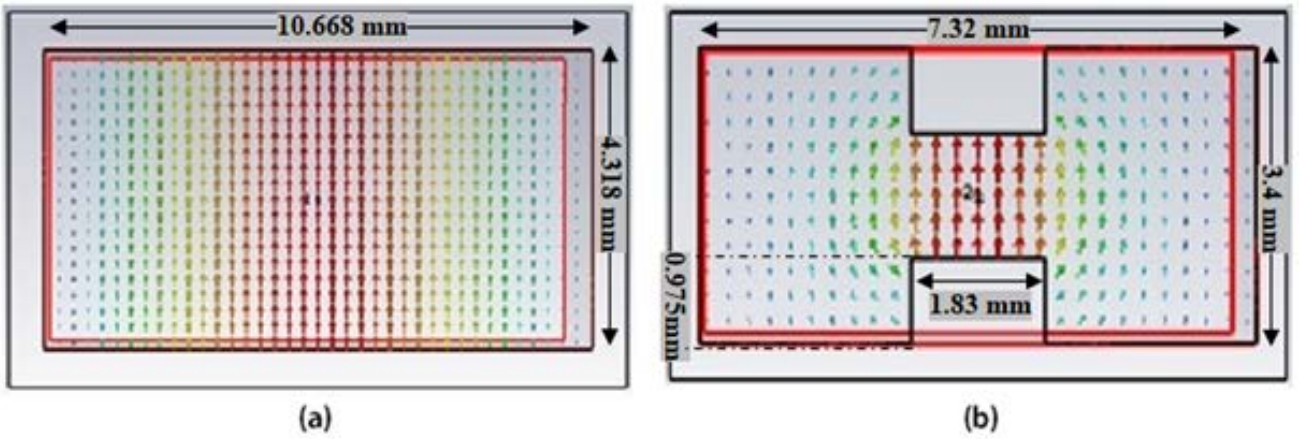

FIGURE 1. Electric field distribution of conventional waveguide (a), and electric field distribution of ridge waveguide (b).

by the ridge waveguide increases the interaction resolution with the inner structure of the inspected dielectric materials.

This paper proposes a microwave NDT technique based on a ridge waveguide and inverse discrete Fourier transform (IDFT) for delamination evaluation. Moreover, a comparison between the ridge waveguide and OERW is presented in delamination imaging, sizing, and thickness estimation. An estimation of the delamination size and thickness is performed by applying IDFT to the measured complex reflection coefficients and following a time-domain reflectometry (TDR) approach based on maximum peak time-step instead of time arrival or magnitude reduction. Due to the nature of propagation in open-ended waveguides and the closeness of the probe to the scanned objects, the conventional far-field time domain reflectometry method is employed to accommodate the near-field, limited bandwidth, and dispersive conditions. The proposed approach and the obtained results are explained in sections 2 and 3, respectively. Finally, the findings of the obtained results are summarized in the conclusion section.

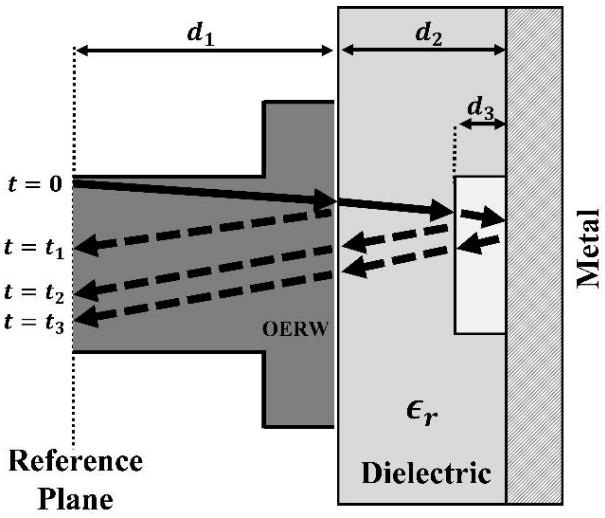

FIGURE 2. Illustration of the pulse reflections' arrangement using an open-ended rectangular waveguide (not drawn to scale).

II. PROPOSED APPROACH

Figure 2 shows a cross-section of the proposed scanning arrangement. Here, an open-ended waveguide with the length of d_1 after the calibration plane is used as a probe. A metal-backed sample that consists of a dielectric layer of d_2 thickness is placed near the waveguide's open end. A d_3-thick delamination is assumed to exist as an air gap between the dielectric layer and the metal directly beneath the location of the OERW. Given a stimulus pulse emerging from the reference plane at the time, $t = 0$, a partial reflection will take place when this wave reaches the discontinuity at the dielectric surface. This reflection will appear at the reference plane at $t = t_1$ as a peak in the reflection coefficient. The remainder of the energy penetrates the dielectric for a distance of $d_2 - d_3$ until encountering the second partial reflection at the edge of the delamination. This reflection gives rise to another peak at $t = t_2$. The rest of the energy will undergo a total reflection at the metallic back end and appear at the reference plane as a third peak at $t = t_3$.

Conventional TDR monitors the variations in time arrival of the reflected waves due to the impedance of discontinuity inside the inspected medium [38]. These variations provide knowledge about the distance differences between every scanned location and the reference plane. However, in the near field inspection, monitoring the time arrival of the reflected waves that usually travelled at light speed is not accurate once using rectangular waveguides [31]. This is because the rectangular waveguides are dispersive transmission lines, and different frequency components travel at different velocities. Therefore, using the reflected waves' time arrival cannot identify the accurate distance to the reflection source.

Instead of time arrival, many TDR techniques are proposed for microwave near field inspection. In [2] and [39], reflection

coefficients obtained using OERW are converted into time-domain using inverse fast Fourier transform (IFFT). After that, the magnitude variation in the second peak corresponding t_2 is monitored to illustrate the variation between the defect and defect-free locations. The delamination in composite insulation is observed based on the magnitude variations of the second peak. These variations indicate a linear relationship between the magnitude of the second peak and the dielectric thickness before the delamination. Despite the promising results of delamination detection, the detected delamination's size and depth cannot be evaluated accurately. In IFFT-based TDR, the time domain reflection can only be measured at discrete time steps of $1/BW$.

In [31], a TDR approach is proposed based on calculating the IDFT using the full form below [40].

$$F(\tau) = \sum_{n=0}^{N-1} F(\nu)\, e^{j2\pi(\frac{\nu}{N})\tau} \tag{1}$$

where $\frac{\nu}{N}$ is analogous to the frequency in sample per cycle, τ is the discrete-time increment, and $F(\nu)$ is the discrete frequency data set. IFFT is an efficient way to implement (1), where the time domain data is found at discrete points separated by $1/BW$. Using (1), however, allows finding the reflection coefficient at any time instant. Therefore, using IDFT, the number of time steps could be extended from 101 to 1000. This process can be considered artificially increasing the measurement bandwidth by adding zeroes to the measured data. In other words, the time step ($1/BW$) is reduced by oversampling the time domain data. This enhances the chance of detecting the shifts in the pulses' peaks reflected back from the internal defects. Therefore, the time-step of the second peak is recorded instead of the magnitude coefficient. The thickness of delamination is observed through the time-step variations of the second peak correlated to the thickness variations using OERW. However, the variations in the second peak's magnitude and time-step cannot always accurately measure delamination thickness. Further analysis is required to select a suitable peak, especially once a different waveguide is used.

In the TDR approach based on implementing (1), a waveguide operated using a wider bandwidth, such as a ridge waveguide, provides more narrow pulses than OERW that makes the second main peak's information inadequate for delamination detection and thickness evaluation. This research's proposed method relies on observing the time-step of the maximum peak reflection to overcome this limitation. The maximum peak reflection refers to the maximum interaction response from the inspected material, which can be easily detected and analyzed among the other reflected peaks. Compared to the delamination-free location, the maximum peak's time-step varies in proportion to the insulation's delamination thickness. This variation in the time-step of the maximum peak is recorded and used to estimate the delamination thickness (d_{et}) as given in (2).

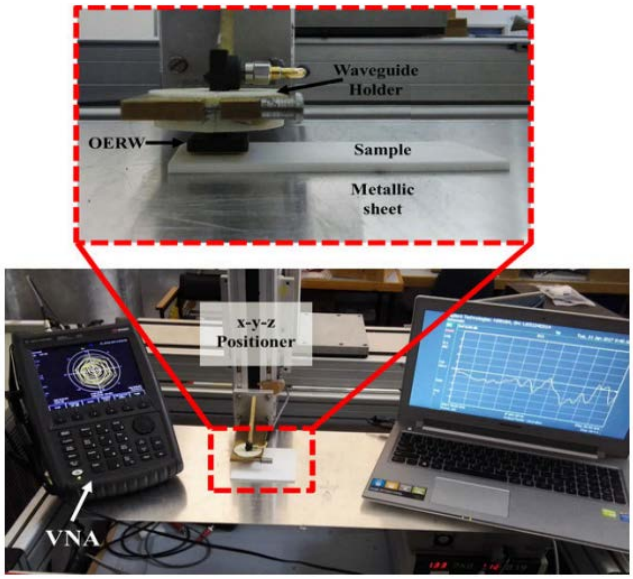

FIGURE 3. Experimental setup of the proposed technique.

$$d_{et} = d_{at} \times \frac{|m_{loc} - m_{ref}|}{100} \tag{2}$$

where d_{at} is the actual thickness of the inspected sample layer. $m_{loc}$is the time-step of the maximum peak of the inspected location. m_{ref} denotes the maximum peak time-step of the defect-free reference.

The error rate of the delamination thickness per measured unit (e.g. mm) is obtained from the difference between the defect's actual thickness and the estimated thickness as given in (3).

$$error = |d_{et} - d_{ac}| \tag{3}$$

where d_{ac} is the actual thickness of the defect.

III. RESULT AND DISCUSSION

An experimental setup is prepared, as shown in Figure 3 to validate the above assumptions. First, a sample is fabricated with artificial defects of different sizes and depths, as shown in Figure 4. This sample is made of a low-loss glass-ceramic (Macor) with a dielectric constant of 5.67 at 8.5 GHz [41]. Next, the sample's back surface is scanned several times using OERW (WR48) and ridge (WRD180) waveguides while the machined surface is placed on metal to simulate the delamination between the insulation and the metal substrate.

A raster scanning is performed with a 1 mm spatial resolution in x and y directions using a programmable xyz-positioner to control the scanning process's waveguide movement. The stand-off distance of 1 mm is set between the end of the probe aperture and the inspected insulation. The complex reflection coefficient is obtained from every scanned location using a portable Vector Network Analyzer (VNA) by linear frequency sweeping with 101 frequency points for each probe's frequency range, as shown in Table 1. One port

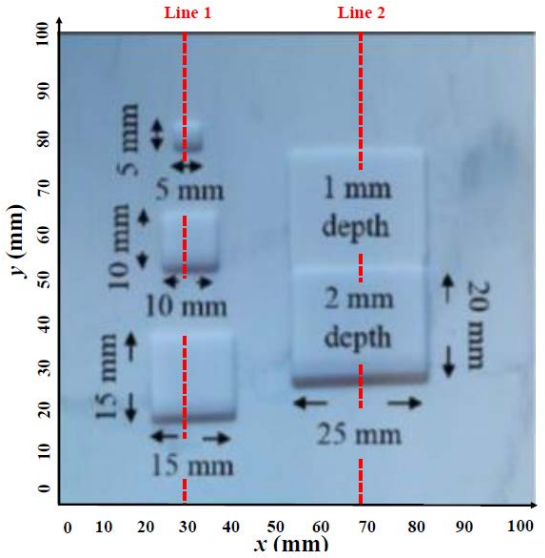

FIGURE 4. A photograph of the fabricated Macor sample.

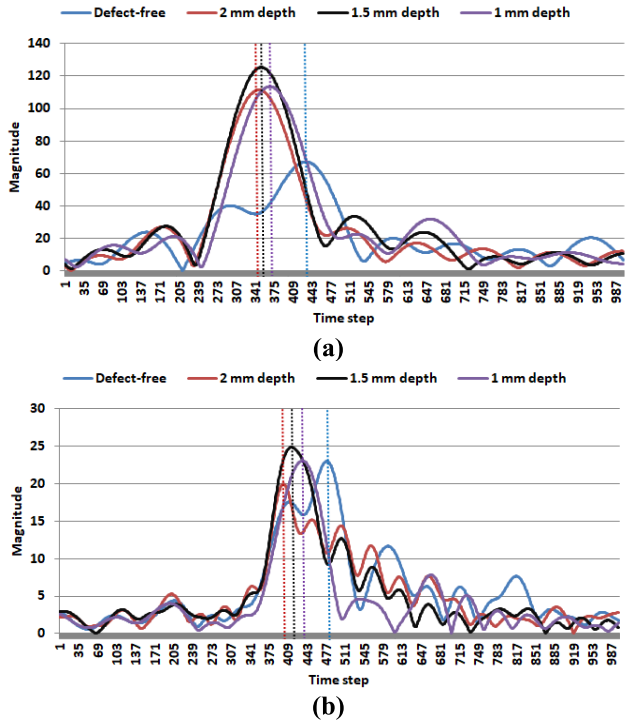

FIGURE 5. IDFT result of the measured reflection coefficient at several defects and defect-free locations using WR42 (a), WRD180 (b).

calibration with 2.40 mm microwave cable is connected with three well-known standard Open-Short-50 Ω Load (OSL) to mitigate the calibration errors between the VNA and the waveguides. This tuning will bring the reference plane to the waveguide's input port, which is much simpler and preferable for discontinuity inspection.

Figure 5 shows the magnitude of the reflection coefficients obtained from the middle of every defect shown in Figure 4 compared to the defect-free locations after converting them into the time domain using IDFT. The obtained references show multiple pulses along with the 1000 time steps in both used waveguides. It can be observed that the waveguide operated using a narrow bandwidth such as WR42 leads to a broader pulse form, as shown in Figure 5(a). The wide pulse form refers to a limited bandwidth resolution of the WR42 waveguide during the interaction with the inspected sample. On the other hand, the large bandwidth operated by the WRD180 waveguide provides a narrow pulse, which refers to increasing the inspection resolution, as shown in Figure 5(b). These narrow pulses provide more information about the inspected sample's inner structure, which increases the detection sensitivity of the inner defects.

TABLE 1. Information about the examined waveguides.

Waveguide	WR42	WRD180
Frequency range	18-26.5 GHz	18-40 GHz
Bandwidth	8 GHz	22 GHz
Sweeping step	0.085 GHz	0.22 GHz
Calibration	2.4 mm	2.4 mm
Aperture size	10.668×4.318 = 46.0644 mm^2	7.32×3.40-2×(1.83×0.975) = 21.3195 mm^2

On the other hand, Figure 5(a) shows the reflected microwave signal's magnitude using the WR42 waveguide. In this graph, the peak of interest is the maximum peak which can be easily identified among the other peaks. In terms of delamination detection, the maximum peak amplitude variations are proportional to distinguish between the defect and defect-free locations. The maximum peak magnitude of the defect-free location is significantly smaller than the defected location. However, the magnitude variation is not proportional to the delamination depth, which only provides information about the delamination presence. In the ideal case of delamination depth estimation, the maximum peak's magnitude should be reduced proportionally from the maximum delamination depth followed by a small delamination depth and finally by defect-free reference. In other words, the maximum peak magnitude of 2 mm, 1.5 mm, and 1 mm delamination should be reduced proportionality before the maximum peak of the defect-free reflections, respectively.

Compared to the magnitude results, the WR42 waveguide provides promising results regarding depth variations through the maximum peaks' time-step, as shown in Figure 5(a). The maximum peak's location corresponding to the time-step number shows that the time-step of the delamination obtained from 2mm, 1.5mm, and 1mm ordered before the defect-free location at 348, 352, 367, and 431-time steps, respectively. Moreover, the maximum peak at 352 time-step of 1.5mm delamination is near the middle between the 2mm and 1mm delamination located at 357 time-step with an error rate of 5 time-steps. The maximum peak time-step arrangement

TABLE 2. Delamination depth evaluation using the maximum peak time-step of the defect-free based on WR42 and WRD180 waveguides.

Waveguide	Time-step	Defect size (mm)	25×20	25×20	15×15	10×10	5×5	Overall error rate (%)
		Actual depth (mm)	2	1	1.5	1.5	1.5	
WR42	Defect-free reference at time-step (431)	Depth (mm)	2.41	2.12	2.40	2.47	2.48	64.50%
		Error (mm)	0.41	1.12	0.90	0.97	0.98	
WRD180	Defect-free reference at time-step (478)	Depth (mm)	**2.30**	**1.17**	**1.94**	**1.97**	**1.79**	**22.40%**
		Error (mm)	**0.30**	**0.17**	**0.44**	**0.47**	**0.29**	

provides encouraging results in terms of the delamination depth using (2).

Figure 5(b) shows the reflected microwave signals obtained by the WRD180 waveguide after conversion into the time domain using IDFT. The reflected signals are obtained from the same defect and defect-free reference locations. Compared to WR42 waveguide results, the magnitude of the maximum peak obtained by WRD180 is incapable of providing the delamination presence information due to the insignificant variations of the maximum peak amplitude between the defect and defect-free locations. As a result, these magnitude variations are incapable of estimating the delamination depth variations as well. The encouraged depth estimation can be observed at the maximum peak location corresponding to the time-step line, as shown in Figure 5(b). The delamination's time-steps with 2mm, 1.5mm, 1mm, and defect-free are located at 400, 415, 436, and 478, respectively. The order of the maximum peak's time-step from maximum delamination to the defect-free location is proportional to the level of the delamination depth. The maximum peak at 415 time-step of 1.5 mm delamination closes to the middle between the 2 mm and 1 mm delamination located at 419 time-step with an error rate of 4 time-steps compared to 5 time-steps of WR42 waveguide.

Table 2 summarizes the mean of the estimated depth for all 5 delamination using WR42 and WRD180 waveguides. In-depth estimation, WRD180 waveguide shows promising results based on the time-step variations of the maximum peak compared to WR42 waveguide. WRD180 waveguide achieves the minimum error rate of delamination depth estimation. In the case of the WRD180 waveguide, the time-step variation of the maximum peak is quite proportional to the delamination depth due to the good arrangement of the maximum peaks corresponding to the thickness variations which is clearly shown in Figure 5(b). In the case of the WR42 waveguide, the maximum peak of the defect-free location shown in Figure 5(a) comes far from the peaks of defected locations which degrades the accurate depth estimation. As a result, the delamination depth seems larger than the actual one unless adjusting the time-step of the defect-free reference. Therefore, selecting an alternative time-step of the defect-free maximum peak may provide accurate depth estimation for both waveguides.

The optimal time-step of the defect-free reference m_{ref}^{opt} that can perceive the proper difference to the delamination depth is given in (4). Herein, the optimal time-step works similarly to a threshold value that can provide the best depth prediction based on the information of the 1 mm delamination. This optimal time-step of defect-free reference aims to make the depth error of 1mm delamination reference point equals to zero based on its Small Size Sample (SSS) that may improve the evaluation process. SSS performs a supervised data analysis instead of the massive training sample in various applications, primarily in machine learning techniques [42]–[44]. In this research, SSS is used to check the improvement of the depth estimation once limited knowledge about the delamination is provided.

$$m_{ref}^{opt} = \left| m_{ref} - 2m_{loc} - \frac{100}{d_{at}} \times (d_{et} + d_{ac}) \right| \tag{4}$$

where m_{ref} denotes to the time-step of defect-free reference. m_{loc} refers to the time-step of defect reference. d_{at}, d_{et} and d_{ac} denote to the sample thickness, estimated and actual delamination thickness, respectively.

Table 3 shows the mean of delamination depth after adjusting the time-step of the defect-free reference m_{ref}^{opt}. In case of WR42 waveguide, the optimal time-step reference $m_{ref}^{opt} = 400$ which is capable of estimating the delamination depth variation with an acceptable degree of accuracy based on the information of the small depth delamination reference measured using WR42 waveguide where $m_{ref} = 431$, $m_{loc} = 367$, $d_{at} = 3mm$, $d_{et} = 1.92mm$ and $d_{ac} = 1mm$. The difference between the estimated time-step of the defect-free and the optimal one is based on (4) is 431-400= 31 time-steps which is a large difference that makes the delamination depth larger than the actual one.

In term of the WRD180 waveguide, the optimal time-step of the defect-free reference $m_{ref}^{opt} = 469$ based on (4) where $m_{ref} = 478$, $m_{loc} = 436$, $d_{at} = 3mm$, $d_{et} = 1.26mm$ and $d_{ac} = 1mm$. This optimal time-step perceives a proper difference between the defect-free time-step and the time-step of the small depth delamination. The difference between the estimated time-step of the defect-free and the optimal one is $478 - 469 = 9$ time-steps which is a small difference compared to 31 time-steps of the WR42 waveguide. This small difference reflects the

TABLE 3. Delamination depth evaluation using the optimized time-step reference of the defect-free based on WR42 and WRD180 waveguides.

Waveguide	Time-step	Defect size (mm)	25×20	25×20	15×15	10×10	5×5	Overall error rate (%)
		Actual depth (mm)	2	1	1.5	1.5	1.5	
WR42	Optimized defect-free reference at time-step (400)	Depth (mm)	1.48	1.20	**1.47**	**1.55**	**1.57**	11.20%
		Error (mm)	0.52	0.20	**0.03**	**0.05**	**0. 07**	
WRD180	Optimized defect-free reference at time-step (469)	Depth (mm)	**1.94**	**0.81**	1.58	1.61	**1.43**	**7.87%**
		Error (mm)	**0.06**	**0.19**	0.08	0.11	**0.07**	

TABLE 4. Delamination size evaluation using the maximum peak time-step of the defect-free based on WR42 and WRD180 waveguides.

Waveguide	Time step	Defect depth (mm)	Starting point	Ending point	Estimated size (mm)	Actual size (mm)	Error	Overall means error
WR42	Defect-free reference at time-step (431)	2	16	42	27	20	35%	53%
		1	43	60	18	20	10%	
		1.5	11	31	21	15	40%	
		1.5	36	51	16	10	60%	
		1.5	56	66	11	5	120%	
	Defect-free reference at time-step (400)	2	17	38	22	**20**	**10%**	20%
		1	39	58	20	**20**	**0%**	
		1.5	13	30	18	15	20%	
		1.5	38	50	13	10	30%	
		1.5	58	64	7	5	40%	
WRD 180	Defect-free reference at time-step (478)	2	14	36	23	20	15%	16.3%
		1	37	54	18	20	10%	
		1.5	9	27	19	15	26. 7%	
		1.5	34	46	13	10	30%	
		1.5	55	59	5	**5**	**0%**	
	Defect-free reference at time-step (469)	2	14	35	22	**20**	**10%**	**5%**
		1	36	54	19	20	5%	
		1.5	11	25	15	**15**	**0%**	
		1.5	35	45	11	**10**	**10%**	
		1.5	55	59	5	**5**	**0%**	

significant measurement of the WRD180 waveguide in terms of delamination depth estimation, as shown in Table 3. WRD180 waveguide achieves the minimum overall error rate of delamination depth estimation. In the case of the WRD180 waveguide, the error rate in delamination depth based on the maximum peak time-step is 22.40% compared to 64.50% using the WR42 waveguide. These error rates are significantly reduced to 11.20% and 7.87% by the optimized time-steps in WR42 and WRD180 waveguides.

Figure 6 shows the imaging results with delamination depth based on colour map variations of the Macor sample using WR42 and WRD180 waveguides. Figure 6(a) illustrates the variations in delamination depth based on the data of the WR42 waveguide processed using (2). The depth of all delamination seems hugely higher than the actual values. After optimizing the maximum peak time-step of defect-free location using (4), all delamination with 1.5mm depth seems closer to the actual depth value, as shown in

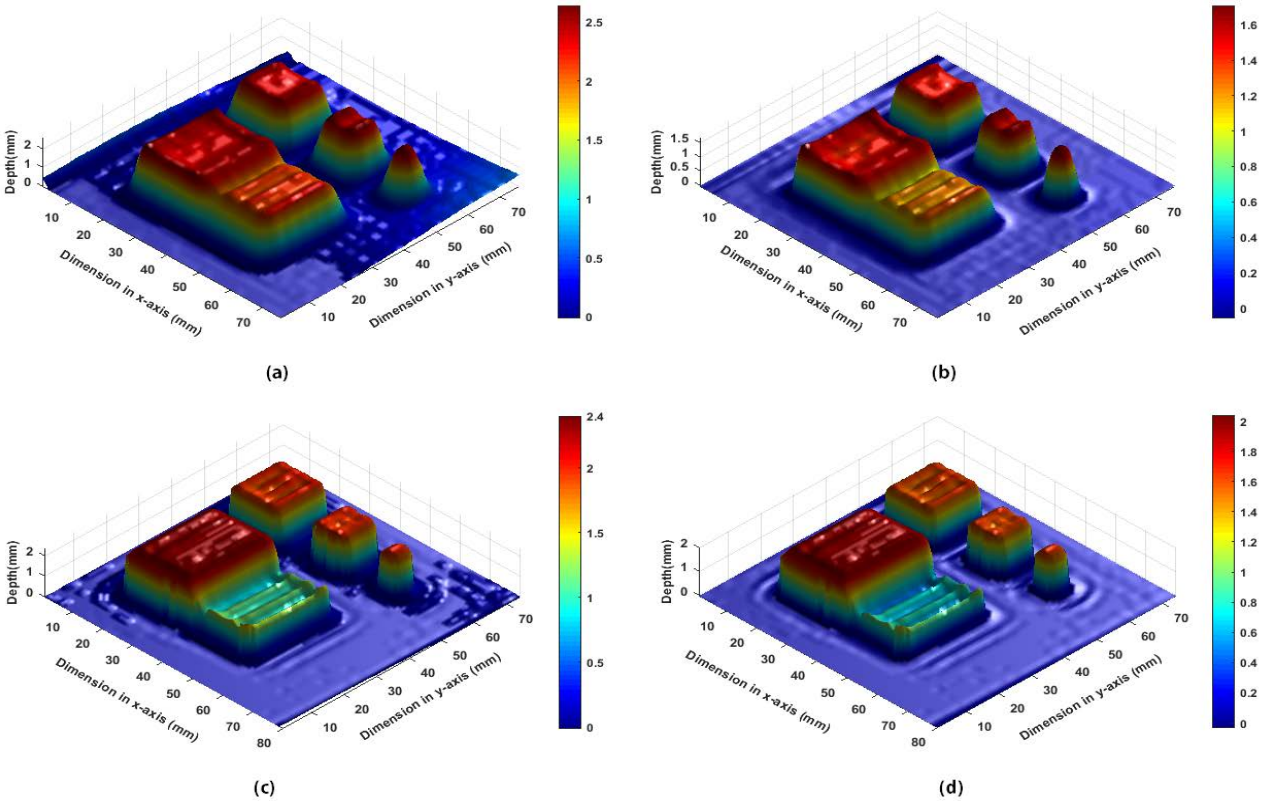

FIGURE 6. Imaging results based on WR42 at 431 time-step (a), WR42 at 400 time-step (b), WRD180 at 478 time-step (c), and WRD180 at 469 time-step (d).

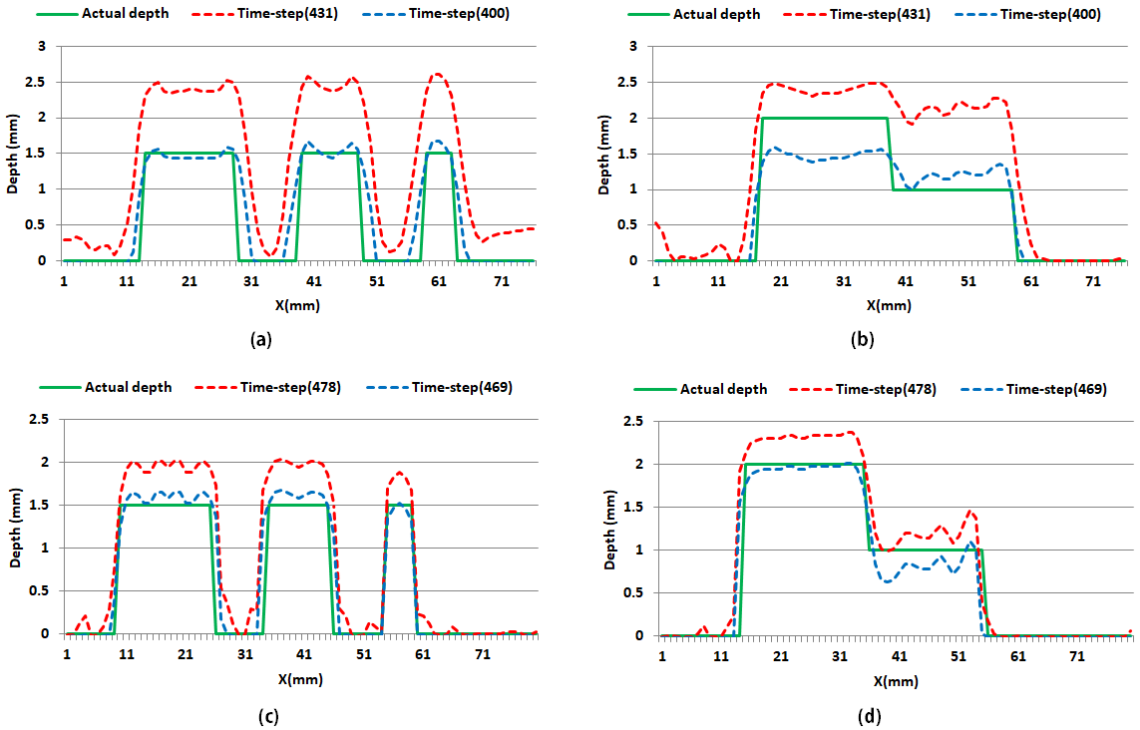

FIGURE 7. Illustration of delamination depth and size variations using WR42 at line 1 (a), WR42 at line 2 (b), WRD180 at line 1 (c), and WRD180 at line 2 (d).

Figure 6(b). The delamination with 1mm depth is reduced near to its actual value compared to the same delamination processed using (2). However, the delamination with 2mm depth is highly reduced near 1.48mm depth. On the other hand, Figure 6(c) shows the imaging results of the WRD180 waveguide processed using (2). Again, the depth of all delamination is higher than their actual values compared to the same data obtained by the WR42 waveguide. This difference is optimized once the acquired data is processed using (4) as shown in Figure 6 (d).

Figure 7 shows a comparison between the actual delamination size and the estimated one obtained from lines 1 and 2, as shown in Figure 4. According to the maximum peak reference results at 431 time-step, the delamination's size seems significantly larger than the actual size along both lines once the WR42 waveguide is used, as shown in Figure 7(a) and(b). The delamination is not sharply separated due to the large aperture size of the WR42 waveguide which its inner dimensions are 10.668×4.318 mm^2. Nevertheless, the size of the delamination is reduced significantly using the optimized reference at 400 time-step. However, the delamination along line 2 are not well separated, as shown in Figure 7(b). The promising results regarding the delamination size are obtained using the WRD180 waveguide as shown in Figure 7(c) and (d). The lateral delamination's size is adequately fitted with the actual size at 478 time-step even before using the optimized time-step. Moreover, the optimized reference at 469 time-step quietly improves the size of the delamination in both lines. All delamination were sharply separated compared to WR42 measurement.

Table 4 shows the numerical analysis of delamination size using both waveguides. The size of delamination is obtained along the x-axis as shown in Figure 7 with 0.5 depth threshold for eliminating the small thickness variations near to zero value. The estimated size of delamination is measured by counting the inspected locations between the starting and ending boundaries of the defect in the millimetre unit. Compared to the actual size, the WR42 waveguide based on the information of 431 time-step is the worst in delamination sizing with 53% of the overall error rate. This error rate is highly reduced by 33% once the delamination size is obtained using the information of 400 time-step. Compared to the WR42 waveguide, WRD 180 has performed an acceptable degree of sizing accuracy with 16.3% of overall error rate once the features are extracted using 478 time-step. This error rate is significantly reduced down to 5% only once the information of 469 time-step is used. The operating frequency range with a small aperture size of WRD 180 makes it possible for providing a reliable inspection for composite materials with an acceptable degree of accuracy in terms of delamination size and depth. Considering the aforementioned discussion, WRD 180 waveguide based on the maximum peak's time-step and its optimization has significantly outperformed the conventional W42 probe.

IV. CONCLUSION

In this paper, a microwave TDR-based NDT technique has been proposed. This method relies on taking the IDFT for the measured complex reflection coefficient at dielectric samples' surface with machined delamination. Using this process, each reflected pulse is allowed to reach its maximum value in the time domain. Using two types of waveguide probes, namely WR42 and WRD 180, it has been shown that it is possible to estimate the delamination size and depth by tracking the time-step of the maximum peak. Unlike conventional arrival time or peak amplitude-based TDR, the proposed technique provides a close estimation for delamination depth using both waveguides by optimizing the defect-free time-step based on the small size sample of 1 mm delamination depth.

Moreover, a comparison has been made between the two waveguides used to implement the proposed technique. It has been shown that the WRD180 waveguide provides the best accuracy performance with a minimum error rate of 7.87% and 5% in terms of delamination depth and size, respectively, compared to the WR42 waveguide. The results reported in this paper prove the superiority of the proposed TDR-based microwave NDT using ridge waveguides over the previously reported techniques, where the narrow bandwidths of the waveguide probes highly affect the delamination depth estimation. Hence, the proposed technique provides a vital tool for many industries, such as inspecting turbine blades' insulation in the aerospace industry, where estimating dielectric coating delamination thickness is of great importance for early defect detection, sizing and depth evaluation.

REFERENCES

[1] M. F. Akbar, R. Sloan, C. I. Duff, M. Wielgat, and J. F. Knowles, "Microwave nondestructive evaluation of thermal barrier coated turbine blades using correlation analysis," in *Proc. 46th Eur. Microw. Conf.*, 2016, pp. 520–523, doi: 10.1109/EuMC.2016.7824394.

[2] M. F. Akbar, G. N. Jawad, L. R. Danoon, and R. Sloan, "Delamination detection in glass-fibre reinforced polymer (GFRP) using microwave time domain reflectometry," in *Proc. 15th Eur. Radar Conf. (EuRAD)*, Sep. 2018, pp. 253–256, doi: 10.23919/EuRAD.2018.8546540.

[3] Z. Li, A. Haigh, C. Soutis, A. Gibson, and P. Wang, "A review of microwave testing of glass fibre-reinforced polymer composites," *Nondestruct. Test. Eval.*, vol. 34, no. 4, pp. 429–458, Oct. 2019, doi: 10.1080/10589759.2019.1605603.

[4] N. H. Hadi and B. J. Hamood, "Vibration analysis of a composite plate with delamination," *J. Eng.*, vol. 21, pp. 144–164, Apr. 2015.

[5] Z. Tian, L. Yu, and C. Leckey, "Delamination detection and quantification on laminated composite structures with Lamb waves and wavenumber analysis," *J. Intell. Mater. Syst. Struct.*, vol. 26, no. 13, pp. 1723–1738, Sep. 2015, doi: 10.1177/1045389X14557506.

[6] F. Gao, L. Zeng, J. Lin, and Y. Shao, "Damage assessment in composite laminates via broadband Lamb wave," *Ultrasonics*, vol. 86, pp. 49–58, May 2018, doi: 10.1016/j.ultras.2018.01.005.

[7] B. Ji, Q. Zhang, J. Cao, H. Li, and B. Zhang, "Non-contact detection of delamination in stainless steel/carbon steel composites with laser ultrasonic," *Optik*, vol. 226, Jan. 2021, Art. no. 165893, doi: 10.1016/j.ijleo.2020.165893.

[8] P. G. Bison, S. Marinetti, E. G. Grinzato, V. P. Vavilov, F. Cernuschi, and D. Robba, *Inspecting Thermal Barrier Coatings by IR Thermography*, K. E. Cramer and X. P. Maldague Eds. Bourne, U.K.: Thermosense, 2003, p. 318, doi: 10.1117/12.486019.

[9] J. Wang, J. Zhang, T. Chang, L. Liu, and H.-L. Cui, "Terahertz nondestructive imaging for foreign object detection in glass fibre-reinforced polymer composite panels," *Infr. Phys. Technol.*, vol. 98, pp. 36–44, May 2019, doi: 10.1016/j.infrared.2019.02.003.

[10] J. White, G. Fichter, A. Chernovsky, J. F. Whitaker, D. Das, T. M. Pollock, D. Zimdars, D. O. Thompson, and D. E. Chimenti, "Time domain terahertz non-destructive evaluation of aeroturbine blade thermal barrier coatings," in *Proc. AIP Conf.*, 2009, pp. 434–439, doi: 10.1063/1.3114273.

[11] C.-C. Chen, D.-J. Lee, T. Pollock, and J. F. Whitaker, "Pulsed-terahertz reflectometry for health monitoring of ceramic thermal barrier coatings," *Opt. Exp.*, vol. 18, no. 4, p. 3477, Feb. 2010, doi: 10.1364/OE.18.003477.

[12] M. K. Hinders, M. K. Hinders, and C. A. Miller, *Intelligent Structural Health Monitoring With Ultrasonic Lamb Waves*. 2020, doi: 10.1007/978-3-030-49395-0_2.

[13] N. H. M. M. Shrifan, M. F. Akbar, and N. A. M. Isa, "Prospect of using artificial intelligence for microwave nondestructive testing technique: A review," *IEEE Access*, vol. 7, pp. 110628–110650, 2019, doi: 10.1109/ACCESS.2019.2934143.

[14] F. Ciampa, P. Mahmoodi, F. Pinto, and M. Meo, "Recent advances in active infrared thermography for non-destructive testing of aerospace components," *Sensors*, vol. 18, no. 2, p. 609, Feb. 2018, doi: 10.3390/s18020609.

[15] H. Seidfaraji, M. I. Fuks, C. Christodoulou, and E. Schamiloglu, "Efficient power combiner for THz radiation," *AIP Adv.*, vol. 6, no. 8, Aug. 2016, Art. no. 085220, doi: 10.1063/1.4962150.

[16] K. Brinker, M. Dvorsky, M. T. Al Qaseer, and R. Zoughi, "Review of advances in microwave and millimetre-wave NDT&E: Principles and applications," *Phil. Trans. Roy. Soc. A, Math., Phys. Eng. Sci.*, vol. 378, no. 2182, Oct. 2020, Art. no. 20190585, doi: 10.1098/rsta.2019.0585.

[17] N. H. M. M. Shrifan, M. F. Akbar, and N. A. Mat Isa, "Maximal overlap discrete wavelet-packet transform aided microwave nondestructive testing," *NDT E Int.*, vol. 119, Apr. 2021, Art. no. 102414, doi: 10.1016/j.ndteint.2021.102414.

[18] M. F. Akbar, R. Sloan, C. I. Duff, M. Wielgat, and J. F. Knowles, "Nondestructive testing of thermal barrier coated turbine blades using microwave techniques," *Mater. Eval.*, vol. 74, pp. 543–551, Apr. 2016.

[19] Z. Li, A. Haigh, C. Soutis, A. Gibson, and R. Sloan, "Applications of microwave techniques for aerospace composites," in *Proc. IEEE Int. Conf. Microw., Antennas, Commun. Electron. Syst.*, Oct. 2017, pp. 1–4, doi: 10.1109/COMCAS.2017.8244755.

[20] N. H. M. M. Shrifan, G. N. Jawad, N. A. M. Isa, and M. F. Akbar, "Microwave nondestructive testing for defect detection in composites based on K-means clustering algorithm," *IEEE Access*, vol. 9, pp. 4820–4828, 2021, doi: 10.1109/ACCESS.2020.3048147.

[21] Z. Li, A. Haigh, C. Soutis, A. Gibson, and R. Sloan, "Microwaves sensor for wind turbine blade inspection," *Appl. Composite Mater.*, vol. 24, no. 2, pp. 495–512, Apr. 2017, doi: 10.1007/s10443-016-9545-9.

[22] S. Mukherjee, X. Shi, L. Udpa, S. Udpa, Y. Deng, and P. Chahal, "Design of a split-ring resonator sensor for near-field microwave imaging," *IEEE Sensors J.*, vol. 18, no. 17, pp. 7066–7076, Sep. 2018, doi: 10.1109/JSEN.2018.2852657.

[23] B. Salski, W. Gwarek, and P. Korpas, "Electromagnetic inspection of carbon-fiber- reinforced polymer composites with coupled spiral inductors," *IEEE Trans. Microw. Theory Techn.*, vol. 62, no. 7, pp. 1535–1544, Jul. 2014, doi: 10.1109/TMTT.2014.2325537.

[24] M. F. Akbar, G. N. Jawad, C. I. Duff, and R. Sloan, "Porosity evaluation of in-service thermal barrier coated turbine blades using a microwave nondestructive technique," *NDT E Int.*, vol. 93, pp. 64–77, Jan. 2018, doi: 10.1016/j.ndteint.2017.09.015.

[25] C. Viegas, B. Alderman, P. G. Huggard, J. Powell, K. Parow-Souchon, M. Firdaus, H. Liu, C. I. Duff, and R. Sloan, "Active millimeter-wave radiometry for nondestructive Testing/Evaluation of composites—Glass fiber reinforced polymer," *IEEE Trans. Microw. Theory Techn.*, vol. 65, no. 2, pp. 641–650, Feb. 2017, doi: 10.1109/TMTT.2016.2625785.

[26] C. Viegas, B. Alderman, P. G. Huggard, J. Powell, A. J. K. M. Firdaus, K. Parow-Souchon, H. Liu, C. I. Duff, and R. Sloan, "Active imaging of glass fiber reinforced plastic using millimeter-wave radiometry," in *Proc. 46th Eur. Microw. Conf.*, Oct. 2016, pp. 73–75, doi: 10.1109/EuMC.2016.7824280.

[27] R. Sutthaweekul, G. Tian, Z. Wang, and F. Ciampa, "Microwave open-ended waveguide for detection and characterisation of FBHs in coated GFRP pipes," *Compos. Struct.*, vol. 225, Oct. 2019, Art. no. 111080, doi: 10.1016/j.compstruct.2019.111080.

[28] M. D. Buhari, G. Y. Tian, and R. Tiwari, "Microwave-based SAR technique for pipeline inspection using autofocus range-Doppler algorithm," *IEEE Sensors J.*, vol. 19, no. 5, pp. 1777–1787, Mar. 2019, doi: 10.1109/JSEN.2018.2879348.

[29] T. W. Siang, M. F. Akbar, G. N. Jawad, T. S. Yee, andM. I. S. Sazali, "A past, present, and prospective review on microwave nondestructive evaluation of composite coatings," *Coatings*, vol. 11, no. 8, p. 913, Jul. 2021, doi: 10.3390/coatings11080913.

[30] N. H. M. M. Shrifan, M. F. Akbar, and N. A. M. Isa, "An adaptive outlier removal aided k-means clustering algorithm," *J. King Saud Univ.-Comput. Inf. Sci.*, pp. 1–12, Jul. 2021, doi: 10.1016/j.jksuci.2021.07.003.

[31] M. F. Akbar, G. N. Jawad, L. D. Rashid, and R. Sloan, "Nondestructive evaluation of coatings delamination using microwave time domain reflectometry technique," *IEEE Access*, vol. 8, pp. 114833–114841, 2020, doi: 10.1109/ACCESS.2020.3003829.

[32] N. J. Lehman, "Constitutive parameter measurement using double ridge waveguide," Ph.D. dissertation, Air Force Inst. Technol., Wright-Patterson AFB, OH, USA, 2013, pp. 1–69. [Online]. Available: https://scholar.afit.edu/etd/882

[33] M. W. Hyde, M. J. Havrilla, A. E. Bogle, and N. J. Lehman, "Broadband characterization of materials using a dual-ridged waveguide," *IEEE Trans. Instrum. Meas.*, vol. 62, no. 12, pp. 3168–3176, Dec. 2013, doi: 10.1109/TIM.2013.2270050.

[34] M. W. Hyde and M. J. Havrilla, "A clamped dual-ridged waveguide measurement system for the broadband, nondestructive characterization of sheet materials," *Radio Sci.*, vol. 48, no. 5, pp. 628–637, Sep. 2013, doi: 10.1002/rds.20044.

[35] M. W. Hyde and M. J. Havrilla, "A broadband, nondestructive microwave sensor for characterizing magnetic sheet materials," *IEEE Sensors J.*, vol. 16, no. 12, pp. 4740–4748, Jun. 2016, doi: 10.1109/JSEN.2016.2548560.

[36] M. W. Hyde and M. J. Havrilla, "Simple, broadband material characterization using dual-ridged waveguide to rectangular waveguide transitions," *IEEE Trans. Electromagn. Compat.*, vol. 56, no. 1, pp. 239–242, Feb. 2014, doi: 10.1109/TEMC.2013.2274898.

[37] J. G. Crosby, M. W. Hyde, and M. J. Havrilla, "Multi-mode analysis of dual ridged waveguide systems for material characterization," in *Proc. USNC-URSI Radio Sci. Meeting*, Jul. 2015, pp. 1–5, doi: 10.1109/USNC-URSI.2015.7303317.

[38] O. Mahdiyar, A. H. Mazinan, M. A. Pourmina, and M. Naser-Moghaddasi, "Super-resolution time domain reflectometry method for microwave imaging system applications," *IETE J. Res.*, vol. 4, pp. 1–11, Apr. 2019, doi: 10.1080/03772063.2019.1604177.

[39] G. N. Jawad and M. F. Akbar, "IFFT-based microwave non-destructive testing for delamination detection and thickness estimation," *IEEE Access*, vol. 9, pp. 98561–98572, 2021, doi: 10.1109/ACCESS.2021.3095105.

[40] J. P. Dunsmore, *Handbook of Microwave Component Measurements*. Chichester, U.K.: Wiley, 2012.

[41] *Macor*, Corning, Corning, NY, USA, 2009.

[42] P. Kokol, M. Kokol, and S. Zagoranski, "Machine learning on small size samples: A synthetic knowledge synthesis," 2021, *arXiv:2103.01002*.

[43] Y. Chu and Y. Zhao, "Bidirectional feature selection with global and local structure preservation for small size samples," *Cognit. Syst. Res.*, vol. 52, pp. 756–764, Dec. 2018, doi: 10.1016/j.cogsys.2018.09.009.

[44] A. Vabalas, E. Gowen, E. Poliakoff, and A. J. Casson, "Machine learning algorithm validation with a limited sample size," *PLoS ONE*, vol. 14, no. 11, Nov. 2019, Art. no. e0224365, doi: 10.1371/journal.pone.0224365.

MUHAMMAD FIRDAUS AKBAR (Member, IEEE) received the B.Sc. degree in communication engineering from International Islamic University Malaysia (IIUM), Malaysia, in 2010, and the M.Sc. and Ph.D. degrees from The University of Manchester, Manchester, U.K., in 2012 and 2018, respectively. From 2010 to 2011, he was with Motorola Solutions, Pulau Pinang, Malaysia, as a Research and Development Engineer. From 2012 to 2014, he was an Electrical Engineer with Usains Infotech Sdn Bhd, Penang, Malaysia. He is currently a Senior Lecturer with Universiti Sains Malaysia (USM). His current research interests include electromagnetics, microwave nondestructive testing, and microwave sensor and imaging.

NAWAF H. M. M. SHRIFAN received the bachelor's degree in computer science and engineering from the University of Aden, Aden, Yemen, in 2006, and the M.Sc. and Ph.D. degrees from Universiti Sains Malaysia (USM), Malaysia, in 2017 and 2022, respectively. He is currently an Assistant Professor with the Department of Oil and Gas Engineering, Faculty of Oil and Minerals, University of Aden. His current research interests include microwave nondestructive testing and computational intelligence algorithms.

GHASSAN N. JAWAD (Member, IEEE) was born in Baghdad, Iraq, in 1984. He received the B.Sc. and M.Sc. degrees in electronics and communication engineering from the University of Baghdad, Baghdad, in 2005 and 2009, respectively, and the Ph.D. degree from The University of Manchester, Manchester, U.K., in 2016. From 2006 to 2009, he was with Orascom Telecom Iraq (Zain Iraq later), as a Network Switching Engineer. He is currently a Lecturer at the University of Baghdad. His current research interests include microwave and millimeter-wave passive components, gyrotropic microwave devices, microwave nondestructive testing techniques, and short-range radar systems.

NOR ASHIDI MAT ISA received the B.Eng. degree (Hons.) in electrical and electronic engineering and the Ph.D. degree in electronic engineering (majoring in image processing and artificial neural network) from Universiti Sains Malaysia (USM), in 1999 and 2003, respectively. He is currently a Professor at the School of Electrical and Electronic Engineering, USM. He has published more than 180, 217, and 294 articles indexed in WoS-ISI (H-index 30), SCOPUS (H-index 36), and Google Scholar (H-Index 42), respectively. Due to his outstanding achievement in research, he gained recognition, both national and internationally. His research interests include intelligent systems, image processing, neural networks, computational intelligence, and medical image processing. He was recognized as top 2% researcher in category-Citation Impact in Single Calendar Years 2019 and 2020 by Stanford University, Stanford, CA, USA, in 2019 and 2020, and Top Research Scientist Malaysia (TRSM) by Akademi Sains Malaysia (ASM), in 2020.